Available online at www.sciencedirect.com
ScienceDirect
Journal of Catalysis 253 (2008) 74–90
JOURNAL OF CATALYSIS
www.elsevier.com/locate/jcat

Synthesis, characterization, and catalytic performance of highly dispersed vanadium grafted SBA-15 catalyst

Guoan Du, Sangyun Lim, Mathieu Pinault, Chuan Wang, Fang Fang, Lisa Pfefferle, Gary L. Haller *

Department of Chemical Engineering, Yale University, P.O. Box 208286, New Haven, CT 06520-8286, USA

Received 9 July 2007; revised 23 October 2007; accepted 25 October 2007

Abstract

Vanadium oxide grafted on mesoporous silica SBA-15 has been synthesized using a controlled grafting process. Its structure has been thoroughly investigated using different characterization techniques, including N_2-physisorption, X-ray diffraction, transmission electron microscopy (TEM), Raman spectroscopy, H_2 temperature-programmed reduction, X-ray absorption near-edge structure (XANES), and extended X-ray absorption fine structure (EXAFS). The spectroscopic results revealed that under dehydrated conditions, the grafted vanadium domains are highly dispersed on the SBA-15 surface, composed predominately of isolated VO_4 units with distorted tetrahedral coordination. The suggested $(\equiv SiO)_3V{=}O$ sites on the silica surface include one short bond (∼1.54 Å) and three long bonds (1.74 Å). Methanol oxidation was used as a chemical probe reaction to examine the catalytic properties of these catalysts. At low vanadium loading, the vanadium species grafted on the surface show structural properties similar to those of vanadium-incorporated MCM-41 catalyst. However, the present mesoporous V-SBA-15 catalysts in the oxidation of methanol to formaldehyde show remarkable catalytic performance compared with that of VO_x/SBA-15 catalysts synthesized through a conventional wet impregnation method, which has been attributed to the homogeneous dispersion and uniformity of the catalytic vanadium species achieved on the SBA-15 support with large pore diameter and surface area. The acidic properties of V-SBA-15 was investigated by pyridine temperature-programmed desorption, which indicated the existence of both Lewis and Brönsted acid sites of the surface.

Keywords: Vanadium grafted SBA-15; Methanol oxidation; XRD; Raman; H_2-TPR; TEM; X-ray absorption (XANES and EXAFS)

1. Introduction

Supported vanadium catalysts consisting of a surface vanadium oxide phase on a high-surface area oxide support have been extensively reported to be active and selective for the partial oxidation of hydrocarbons, oxidative dehydrogenation of alkanes to alkenes, selective catalytic reduction of NO_x, and oxidation of SO_2 [1–6]. The catalytic activity largely depends on the dispersion of vanadium [7,8], the metal–support interaction [5,9] and the nature of the vanadium active sites. Isolated tetrahedral vanadium oxide species containing the terminal V=O group have been proposed to be the active sites for many reactions [10–12].

Recent approaches in developing catalysts have used the homogeneous dispersion of metal species on the surface of porous high-surface area supports, such as silica, alumina, titania, and zirconia, as well as the increased stability of active species on a support. Although extensive efforts have been made to control the dispersion on supported catalysts, the development of a simple methodology to prepare highly dispersed vanadium metal oxide with high vanadium loading remains a challenge [13].

Many reports have addressed the synthesis and characterization of supported vanadium oxide species, and the chemical and structural nature of the vanadia on the supports [14–17]. Improved catalytic performance is often attributed to isolated tetrahedral monovanadate (VO_4) species [16,18]. Using the incipient wet impregnation method, the isolated, three-legged $(\equiv SiO)_3V{=}O$ species was found to be the most favorable site at low coverage on SiO_2, Al_2O_3, TiO_2, ZrO_2, and HfO_2 supports [7,10,19]. However, the precise control of vanadium-isolated active site dispersion has not been successfully achieved by this method, resulting in numerous surface species, including polymeric vanadia species and bulk crystalline V_2O_5, even at

* Corresponding author.
E-mail address: gary.haller@yale.edu (G.L. Haller).

0021-9517/$ – see front matter
doi:10.1016/j.jcat.2007.10.019

low V loadings [20,21]. Since the discovery of mesoporous siliceous materials, such as MCM-41, MCM-48, and SBA-15, extensive research efforts have focused on the application of these materials as catalyst supports [22–24]. However, satisfactory single site dispersion still cannot be easily obtained. Through a modified Beck's method, vanadium-incorporated MCM-41 catalysts have been successfully synthesized by atomic substitution of vanadium ions for Si in the mesoporous framework, resulting in a catalyst with homogeneous, isolated vanadium active sites [25–27]. Through characterization with ^{51}V-NMR and X-ray absorption techniques, the vanadium species have been proposed to be in a distorted tetrahedral coordination local environment with a V=O double bond exposed to the pore surface acting as the active sites and three V–O–Si bonds to the silica framework [25,26]. This type of vanadium-incorporated catalyst shows significant advantages in various oxidation reactions, such as methanol oxidation [15] and methane partial oxidation [28]; however, the low vanadium loading that incorporation can achieve limits further increase in the product yields.

Several grafting methods have been widely used to prepare catalysts on supports [29,30]. The chemical vapor deposition (CVD) process using volatile molecular metal precursors [i.e., $O{=}VCl_3$ [31,32], $O{=}V(OC_2H_5)_3$ [9] or $O{=}V(O^iPr)_3$ [32]] to modify the oxide surfaces and provide a way to control the dispersion of the active sites. The gas–solid reactions of these metal complexes with the surface silica yields isolated and uniform vanadium sites [31,32], whose structures were characterized extensively by ^{51}V magic-angle spinning NMR spectroscopy [10,31,33–37] as well as the X-ray absorption spectroscopy (XANES and EXAFS) [38]. The grafted vanadium is proposed to be in a distorted tetrahedral environment with the molecular complex on the surface assigned to $\equiv SiOVOX_2$ [38]. More recently, a novel so-called thermolytic molecular precursor (TMP) method has been developed and used to control active site dispersion at a molecular level [30,39]. In this method, oxygen-rich metal siloxide complexes are grafted onto an oxide support via a protonolysis reaction, followed by low-temperature calcination to remove the remaining hydrocarbons [40].

The new discovery of the family of siliceous mesostructured material SBA-15 achieved by using a triblock copolymer as structure-directing agent under acidic conditions [41,42] has opened new opportunities in the field of heterogeneous catalysis. Mesoporous SBA-15 silica has become a promising oxide support for many catalysts, owing to its high surface area (600–1000 m^2/g) and silanol concentration, allowing the immobilization of active sites with high dispersion. It has a hexagonal array of uniform tubular channels with pore diameters in the range of 5–30 nm, which is much larger than that of MCM-41, allowing much lower diffusion resistance. Moreover, the thick pore wall (31–64 Å) relative to MCM-41 provides high thermal stability and hydrothermal stability. Several studies have used the mesoporous SBA-15 as a support for vanadium species either by the conventional wet impregnation method or the thermalytic molecular precursor route. Recently, a novel controlled grafting process through atomic layer deposition (ALD) has been successfully used to prepare tungsten oxide catalyst supported on SBA-15 mesoporous silica [43]. Herein we report a method of grafting vanadium oxide species onto the surface of mesoporous silica SBA-15 using the method of atomic layer deposition. This grafting approach was performed under strictly anhydrous conditions and in an organic solvent system, to avoid hydrolysis of the metal precursor and aggregation of the vanadia surface species to form oligomers after the grafting process. To gain further insight into the dispersity and the nature of vanadia species on the SBA-15 support, we performed detailed characterization techniques, including N_2-physisorption, X-ray diffraction (XRD), transmission electron microscopy (TEM), Raman spectroscopy, H_2 temperature-programmed reduction, X-ray absorption near-edge structure (XANES), and extended X-ray absorption fine structure (EXAFS). We investigated the catalytic properties by the methanol oxidation reaction and compared them with those of the vanadium catalysts synthesized via conventional wet impregnation and with selected reports in the literature.

2. Experimental

2.1. Catalyst synthesis

Mesoporous siliceous SBA-15 was prepared according to a well-established procedure delineated by Stucky et al. [42] using tetraethylorthosilicate (TEOS) and triblock co-polymer poly(ethylene glycol)–block–poly(propylene glycol)–block–poly(ethylene glycol) $EO_{20}PO_{70}EO_{20}$ (M_{av} = 5800, from Aldrich) as a template agent under acidic conditions. Typically, a solution of $EO_{20}PO_{70}EO_{20}$:HCl:TEOS:H_2O = 2:60:4.25:12 (mass ratio) was prepared by dissolving 4 g of $EO_{20}PO_{70}EO_{20}$ polymer in 80 g of 2 M HCl and 20 g of H_2O under stirring before the addition of 8.8 g of TEOS dropwise. The solution mixture was stirred at 313 K for 20 h and then aged at 373 K in an autoclave for 48 h. After cooling to room temperature, the resulting solid was recovered by filtration, washed in deionized water, and dried under ambient conditions. The predried solid was heated at a constant rate from room temperature to 813 K over 17 h under He and held for 1 h under the same conditions, followed by calcination at 813.2 K for 5 h with air to remove the residual organic template materials, yielding the final mesoporous SBA-15 materials.

The vanadium-grafted SBA-15 catalysts were synthesized following a controlled grafting process through atomic layer deposition (ALD) [43]. The as-calcined SBA-15 sample was suspended in anhydrous toluene (Aldrich, 99%) by refluxing under an inert N_2 atmosphere for 5 h to remove any adsorbed water. The synthesis of the vanadium precursor and the grafting process were performed under an inert nitrogen atmosphere. Commercial oxovanadium(V) chloride (Aldrich) was used to prepare the vanadium precursor solution. Typically, 0.025 ml of oxovadadium(V) chloride (for the 1.4V-SBA-15 sample) was added dropwise via a syringe in 150 ml of toluene at room temperature, followed by the addition of 20 ml of anhydrous ethanol (Aldrich). The mixed solution was refluxed for 8 h with nitrogen bubbled from the bottom of the solution until

the oxovanadium chloride fully reacted with ethanol and the released HCl was dispelled from the system by the nitrogen flow. The solution was then cooled to room temperature. The excess amount of ethanol was distilled from the precursor solution before the pre-prepared SBA-15 toluene suspension (1.0 g of SBA-15) was added, followed by refluxing at 383 K overnight in a N_2 atmosphere. The resulting mixture was cooled, filtered, and washed with anhydrous toluene several times, then dried at room temperature overnight. The unreacted vanadium precursor and byproducts from the grafting reaction were removed by washing with toluene. The as-synthesized sample calcined in the same process as above yielded the final vanadium-grafted SBA-15 catalysts.

The grafting process involved the reaction of $O{=}V(OEt)_3$ with surface silanol groups, causing cleavage of the V–O bond, and readily formed in situ EtOH. The as-formed EtOH could be easily removed from the toluene solvent system in the process of refluxing (383 K) due to its low boiling point, making the grafting step highly favorable. Thus, it is reasonable to assume that the three-legged $(\equiv SiO)_3V{=}O$ species is the most favorable species on the siliceous SBA-15 surface.

The impregnated sample was prepared by the traditional incipient wet impregnation of siliceous SBA-15 or Cab-O-Sil with vanadyl sulfate trihydrate ($VOSO_4{\cdot}3H_2O$, Aldrich 99%) aqueous solution. Then the sample was calcined at 813 K for 3 h under air. The vanadium-incorporated MCM-41 catalyst was synthesized as a comparison material using a modified Beck's method, as described in our previous work [4,26].

2.2. Characterization

2.2.1. Nitrogen physisorption

Nitrogen adsorption–desorption isotherms at 77 K were measured with a Quantachrome Autosorb-3b static volumetric instrument. Before measurement, the samples were outgassed at 573 K to a residual pressure below 10^{-4} Torr. A Baratron pressure transducer (0.001–10 Torr) was used for low-pressure measurements. The specific surface areas were calculated following the BET method [44]. Pore size and pore size distribution were calculated by the BJH method [45] using the desorption isotherm branch.

2.2.2. XRD

The XRD measurements were conducted using a Bruker AXS D8Focus diffractometer ($Cu K\alpha$, $\lambda = 0.15,4$ nm, 40 KV, 30 mA).

2.2.3. X-ray absorption

X-Ray absorption data were collected at the V K edge (5465 eV) according to the method described by Wong et al. [46], using Si (111) as the monochromator crystal at beam line X23B (National Synchrotron Light Source, Brookhaven National Laboratory). Typically, a ca. 100-mg sample was pressed into self-supporting wafers and placed in a stainless steel cell. Incidence and transmission absorbance of the X-ray beam were measured by ion chambers filled with pure nitrogen. EXAFS in the transmission mode was recorded from 200 eV below to 900 eV above the V K edge. The spectra collected were analyzed using the UWXAFS analysis package [47]. The theoretical EXAFS function for vanadium oxide species generated by the FEFF6 program was used to fit the experimental data to calculate the V–O shell coordination numbers [48]. The gas inlet, outlet, and heating and cooling unit allow the in situ treatment of samples and reaction. The hydrated samples were prepared by exposing the vanadium-grafted SBA-15 catalysts in ambient conditions for 3 h. The dehydrated samples were prepared by in situ heating of the sample wafer in ultra-high-purity He at 623 K for 30 min. To test the reducibility and stability of V-SBA-15, the sample was reduced in ultra-high-purity H_2 at 473, 623, and 773 K for 30 min, then reoxidized in air at 773 K for 30 min.

2.2.4. H_2 TPR

The reducibility and the stability of V-SBA-15 and impregnated V/SBA-15 samples were investigated by a TPR technique using a gas chromatograph (Agilent 6890 Plus) with a thermal conductivity detector (TCD). Approximately 50 mg of each sample was loaded into a quartz cell. Before each TPR run, the sample cell was purged by ultra-zero grade air at room temperature; then the temperature was increased to 773 K at a rate of 5 K/min, soaked for 1 h at the same temperature, and cooled to room temperature. This procedure produces a clean surface before the TPR is run. The gas flow was switched to 5 vol% hydrogen balanced by argon. After baseline stabilization, the sample cell was heated at a rate of 5 K/min to 1123 K and held there for 1 h to ensure complete reduction. A frozen acetone trap was installed between the sample cell and the TCD to condense water produced by the sample reduction.

2.2.5. HR-TEM

As a complementary technique, HR-TEM was used to visualize the structure of V-SBA-15. It was performed on a Phillips Tecnai F20 200-kV microscope.

2.2.6. Raman spectroscopy

Raman spectra were recorded using an excitation wavelength of 532 nm on a Jobin Yvon Horiba LabRam instrument equipped with an Olympus confocal microscope. The samples were pressed into wafers and dehydrated at 423 K for overnight to remove surface moisture before each scan. The hydrated samples were prepared through exposure to ambient conditions for 2 h at room temperature. Spectra were collected at different locations of the wafer and averaged to obtain the final spectrum.

2.2.7. ICP analysis

The vanadium content of each sample was measured by ICP at Galbraith Laboratories, Inc.

2.2.8. TPD

The acid site strength and species of V-SBA-15 samples with different vanadium content were estimated by TPD of pyridine. The adsorption temperature of pyridine and the temperature downstream of the gas chromatograph were set at 423 K, to avoid the condensation of pyridine. After 30 min of pyridine adsorption, the physisorbed pyridine was flushed out by

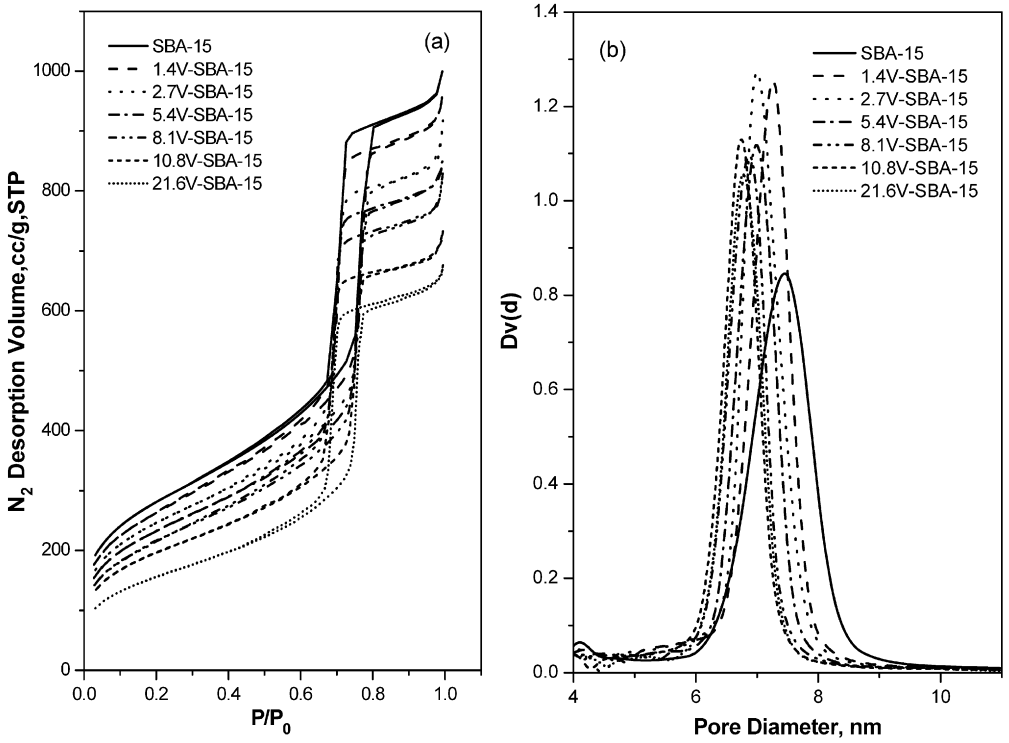

Fig. 1. Nitrogen physisorption of vanadium grafted SBA-15 samples with different vanadium loadings.

a high flow rate of He for 1 h. The temperature was increased to 1123 K at a rate of 5 K/min and held there for 1 h. The signal was collected with a n Agilent 6890 Plus gas chromatograph equipped with a TCD. The carrier gas (He) flow rate was 40 ml/min.

2.3. Catalyst evaluation

In this work, we used the gas-phase partial oxidation of methanol as a probe reaction to evaluate the catalytic performance of the vanadium-grafted catalysts. Typically, a 50-mg catalyst sample was loaded into the quartz reactor, with the thermocouple inserted into the catalyst bed for better control of the actual pretreatment and reaction temperature. The reactor was installed vertically inside a 127-mm-i.d. tubular furnace controlled by a programmable PID temperature controller (Omega CN2011J). All of the gases were controlled by calibrated mass flow controllers (Brooks). The pressure was adjusted with a needle valve and measured on a pressure gauge (Matheson, 0–100 psi). The helium, with constant flow rate controlled by a mass flow controller, was bubbled through a methanol saturator to produce constant concentration of methanol vapor in the feed. Oxygen (2 vol%) balanced with ultra-high-purity helium was used to create a reactant feed mixture of methanol (1.9 vol%), oxygen (2.7 vol%), and helium (95.4 vol%) balance. The downstream of the reactor to the gas chromatograph was heated at 393 K, to avoid condensation of the products. The feed and products were analyzed by an online programmable gas chromatograph (HP 6890) equipped with a TCD, a flame ionization detector with a methanizer, and a Hayesep T column (100/120 mesh 5 ft). Separation of the products and reactants was achieved in a gas chromatograph column with temperature programming. Blank runs were performed on the empty quartz reactor, and no significant conversion of methanol was found.

Before reaction, the catalysts were pretreated in situ in a stream of 10 ml/min ultra-zero grade air at 773 K for 40 min to obtain a clean surface with respect to hydrocarbon contamination. After pretreatment, the catalysts were then flushed with ultra-high-purity He for 20 min. The methanol oxidation was then carried out over a 100-K temperature range (573–673 K) to obtain the conversion, selectivity, and space time yield data.

3. Results and discussion

3.1. Characterization

3.1.1. Nitrogen physisorption

As a primary measurement for the physical properties, nitrogen physisorption was conducted for a series of V-SBA-15 samples with different vanadium loadings (nominal 1.4%–21.6 wt%). The nitrogen adsorption/desorption isotherms and the corresponding pore size distributions are shown in Fig. 1a. All of the vanadium-grafted samples exhibited type IV isotherms with a H_1-type broad hysteresis loop [49], corresponding to a typical large-pore mesoporous materials with 1D cylindrical channels. Capillary condensation of nitrogen with uniform mesopores occurred, causing a sudden step increase in nitrogen uptake in the characteristic relative pressure (P/P_0) range of 0.6–0.8 for all the grafted samples studied, suggesting typical mesoporous structure with uniform pore diameters. Because SBA-15 exhibited a uniform hexagonal array of mesopores connected by smaller micropores, the broad hysteresis loop in the isotherms for all of the vanadium-grafted samples

Table 1
Physical properties of synthesized V-SBA-15 catalysts compared with the blank SBA-15 and various silica supported vanadium catalysts

Sample ID	V-loading (wt%)	Surface density (VO_x/nm^2)	BET (m^2/g)	Pore diameter (nm)	Mesopore volume (cc/g)	Total pore volume (cc/g)
SBA-15	–	–	1024	7.46	1.38	1.54
1.4V-SBA-15	1.4	0.17	956	7.26	1.33	1.47
2.7V-SBA-15	2.8	0.36	899	7.00	1.23	1.43
5.4V-SBA-15	4.8	0.66	847	6.98	1.18	1.32
8.1V-SBA-15	6.1	0.92	783	6.87	1.14	1.30
10.8V-SBA-15	7.0	1.16	716	6.74	1.02	1.15
21.6V-SBA-15	9.2	1.91	569	6.77	0.96	1.08
6.0V/SBA-15	6.0	1.04	679	6.94	1.07	1.21
10.0V/SBA-15	10.0	2.15	550	6.78	0.88	1.15
2.5V-MCM-41	1.5	0.16	1130	2.83	1.00	2.70
$6.0V/SiO_2$	6.0	3.77	188	–	0.03	2.01

is an indication of long mesopores, limiting the emptying and filling of the accessible volume [50]. The amount of nitrogen adsorbed decreased with increasing V content in V-SBA-15. As shown by the pore size distribution in Fig. 1b, the pore size of the catalyst decreased with increasing vanadium loading, with the decrease slowing as the vanadium loading approached monolayer coverage (∼11 wt%).

The physical properties of the series of vanadium-grafted SBA-15 and vanadium-impregnated SBA-15 catalysts, as well as the vanadium-incorporated MCM-41 catalysts, are summarized in Table 1. The BET surface area of the vanadium-grafted samples decreased compared with that of the bare SBA-15. This trend continued with the further increases in V-loading on the surface. Decreases in total volume (from 1.47 to 1.08 cc/g) and mesopore volume (from 1.33 to 0.96 cc/g) and a decline in BET surface area (from 956 to 569 m^2/g) occurred with increasing vanadium loading. The systematic decrease in average pore size from 7.5 to 6.8 nm reflects a homogeneous monolayer covering of the inner pores of SBA-15, which is consistent with the deceased mesopore volumes. The V/SBA-15 samples synthesized by conventional wet impregnation showed smaller BET surface area, lower mesopore volume and lower total pore volume compared with the V-SBA-15 samples with similar V loadings (6.0V/SBA-15 compared with 8.1V-SBA-15; 10.0V/SBA-15 compared with 21.6V-SBA-15). Using Cab-O-Sil as a support of vanadium species ($6.0V/SiO_2$) produced a much higher average surface density of VO_x (3.77 VO_x/nm^2) due to the much lower surface area of SiO_2 (∼200 m^2/g), which resulted in facile surface vanadium aggregation.

3.1.2. XRD

The powder XRD pattern of as-calcined mesoporous silica SBA-15, vanadium-grafted SBA-15, and vanadium-impregnated silica samples are shown in Fig. 2. Typically, the low-angle diffraction pattern shows evidence of three reflections at 2θ values of 0.5°–3°, including one strong peak (100) and two weak peaks (110) and (200), corresponding to a highly ordered hexagonal mesoporous silica framework (Fig. 2a). The vanadium-grafted samples showed the same pattern, indicating that the long-range order of the SBA-15 framework was well retained after the grafting and calcination process. The high-angle diffraction pattern shown in Fig. 2b for the samples with increasing vanadium loading demonstrated no diffraction peaks, excluding the presence of any agglomerate vanadium species on the surface of silica SBA-15 of particle size >ca. 3 nm. This XRD result indicates that not only did the atomic layer deposition by the reaction of the vanadium precursor $(EtO)_3V{=}O$ with the surface hydroxyl groups not result in aggregation of the vanadium to form large particles, but also the vanadium-grafted SBA-15 samples maintained their vanadium surface structure even after the high-temperature (813 K) calcination process. This finding further affirms the high thermal stability of the surface vanadium species. In comparison, XRD features of the impregnated samples (10V/SBA-15 and $6V/SiO_2$), as shown in Fig. 2b, indicate that V_2O_5 crystallites formed during the impregnation. At low vanadium loading for 6V/SBA-15, no significant diffraction peaks indicative of crystallites were seen.

3.1.3. TEM

Fig. 3 compares TEM images obtained from different orientations of vanadium-grafted SBA-15 prepared by different methods. For the low-magnification images shown in Figs. 3a–3c, the TEM images of the bare SBA-15, the vanadium-grafted SBA-15 and the conventional impregnated VO_x/SBA-15 samples all clearly show well-dispersed silica particles with uniform morphology, typically showing a 2-D hexagonal shape with a diagonal of approximately 1 μm (as shown in Figs. 3a–3c for the 8.1V-SBA-15 sample), due to the self-assembly of the tetraethylorthosilicate (TEOS) as the silica source in the process of synthesizing mesoporous SBA-15. The high-magnification TEM images of all of the samples clearly reveal the highly ordered hexagonal arrays of one-dimensional mesopores as a characteristic of SBA-15 support materials, typically represented by 8.1V-SBA-15, as shown in Figs. 3d–3f. These images for the vanadium-supported silica materials prepared by atomic layer deposition clearly show no evidence of bulk V_2O_5 crystallites condensed on the SBA-15 surface, which further confirms that the vanadium species are thoroughly dispersed on the SBA-15 mesopore walls after the grafting process and high-temperature thermal treatment. Figs. 3g–3i show the TEM images for 6.0V/SBA-15 synthesized by wet impregnation. Unlike the vanadium-grafted SBA-15, the samples prepared by impregnation show bulk V_2O_5 crystallites in the framework of

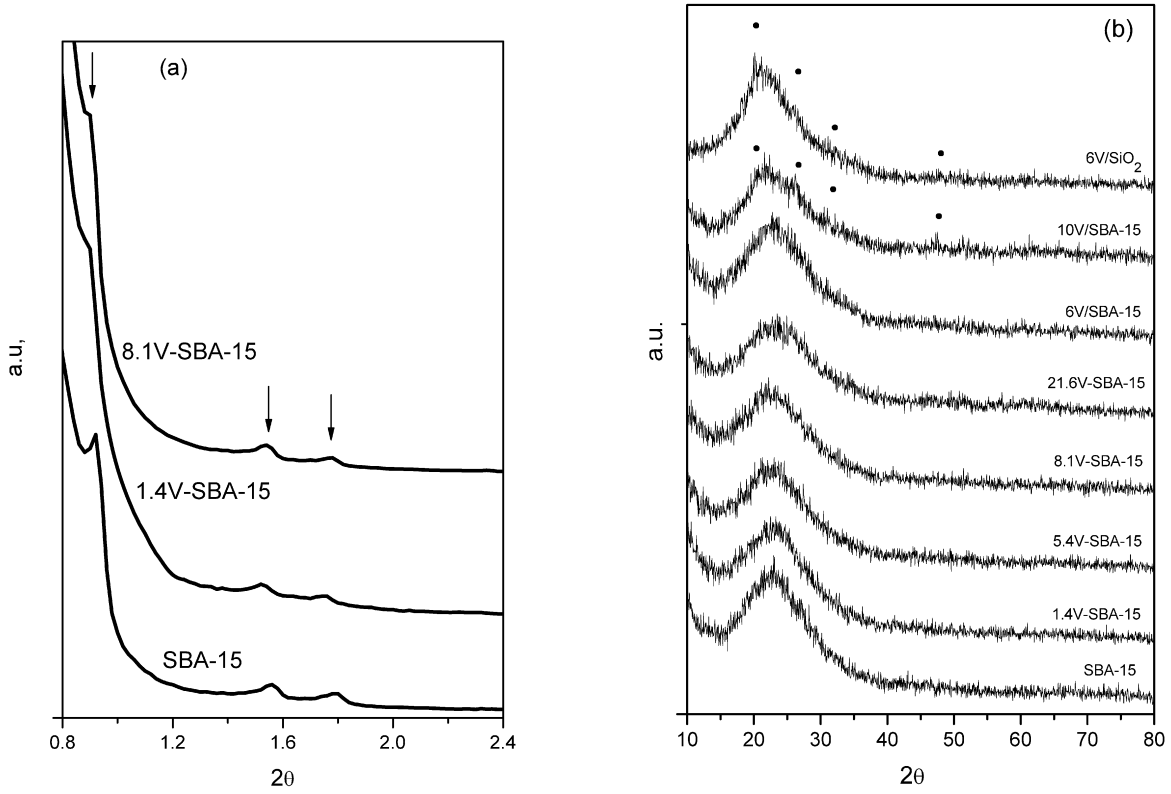

Fig. 2. X-ray diffraction patterns of vanadium grafted SBA-15 at (a) low angle and (b) high angle range.

SBA-15, some of which are large enough (>10 nm) to partially block the pores.

3.1.4. TPR

H_2-TPR is a useful characterization technique for investigating the chemical properties of a metal catalyst. TPR can reveal not only the reducibility and stability of the metal-supported or unsupported catalysts, but also the more profound surface chemical information, that is, metal species, metal distribution, and, even quantitatively, the loading of different metal surface forms. In this study, TPR was carried out between 298 and 1123 K for all of the vanadium-grafted SBA-15 samples with increasing vanadium loading, as shown in Fig. 4. For comparison, the impregnated V/SBA-15 and V/SiO_2 samples, as well as the vanadium-incorporated MCM-41 samples, also were measured. The main feature observed in the V-SBA-15 TPR profiles (Fig. 4a) was a linear increase in the height and width of the reduction peaks for V grafted SBA-15 with increasing vanadium content. A systematic change in the temperature of the maximum reduction rate and of the initial reduction with increasing vanadium content grafted onto the surface of SBA-15 also could be seen. As shown in Fig. 4a, there is a synchronous increase (∼60 K) in temperature from the initial reduction to the maximum reduction rate for all the grafted samples; however, this small shift does not likely mean a change in the surface vanadia structure, but likely is related to the difference in H_2-to-surface vanadia ratio during reduction with increasing vanadium loading.

TPR profiles of the grafted sample (1.4V-SBA-15, 1.4 wt%) and the vanadium-incorporated MCM-41 sample (2.5V-MCM-41, 1.5 wt%) are shown in the inset of Fig. 4b. The V-SBA-15 sample shows only one distinct peak in the range of 673–1123 K, indicating that the samples synthesized by surface grafting are likely to have a single species on the SBA-15 pore surface. The incorporation method for the synthesis of V-MCM-41 allows substitution of the vanadium (+5) into the silica framework of MCM-41 mostly occupying isolated distorted tetrahedral coordination sites with one V=O exposed on the surface of the pore walls and three V–O bonds rooted in the pore walls [25,28]. This allows the presence of both the direct exposed vanadium species and those partially occluded by surface silica, resulting in a distinct peak and a broad shoulder at higher reduction temperatures. In contrast, the atomic layer deposition method used in this study, grafting the vanadium species after the synthesis of the SBA-15 framework (postsynthesis), excludes the partial occlusion effect of the silica; as a result, only distinct peaks can be obtained at lower temperature (∼40 K lower than V-MCM-41 at similar vanadium loadings).

The TPR profiles of the impregnated 6.0V/SiO_2 (6.0 wt%) and 10.0V/SBA-15 (10.0 wt%) sample were compared with those of the V-SBA-15 samples. Clearly, the impregnated 6.0V/SiO_2 sample had a much lower reduction temperature of ca. 638 K, which is 151 K lower than that of the grafted V-SBA-15 sample with similar vanadium loading. This indicates that using the conventional wet impregnation method, aggregated or crystallized V_2O_5 can be formed on the surface of silica (Cab-O-Sil) with low surface area (∼200 m^2/g), resulting in a low reduction temperature. On the other hand, the impregnated V/SBA-15 sample showed similar reduction temperatures (806 K for 6.0V/SBA-15 and 821 K for 10.0V/SBA-15) at a

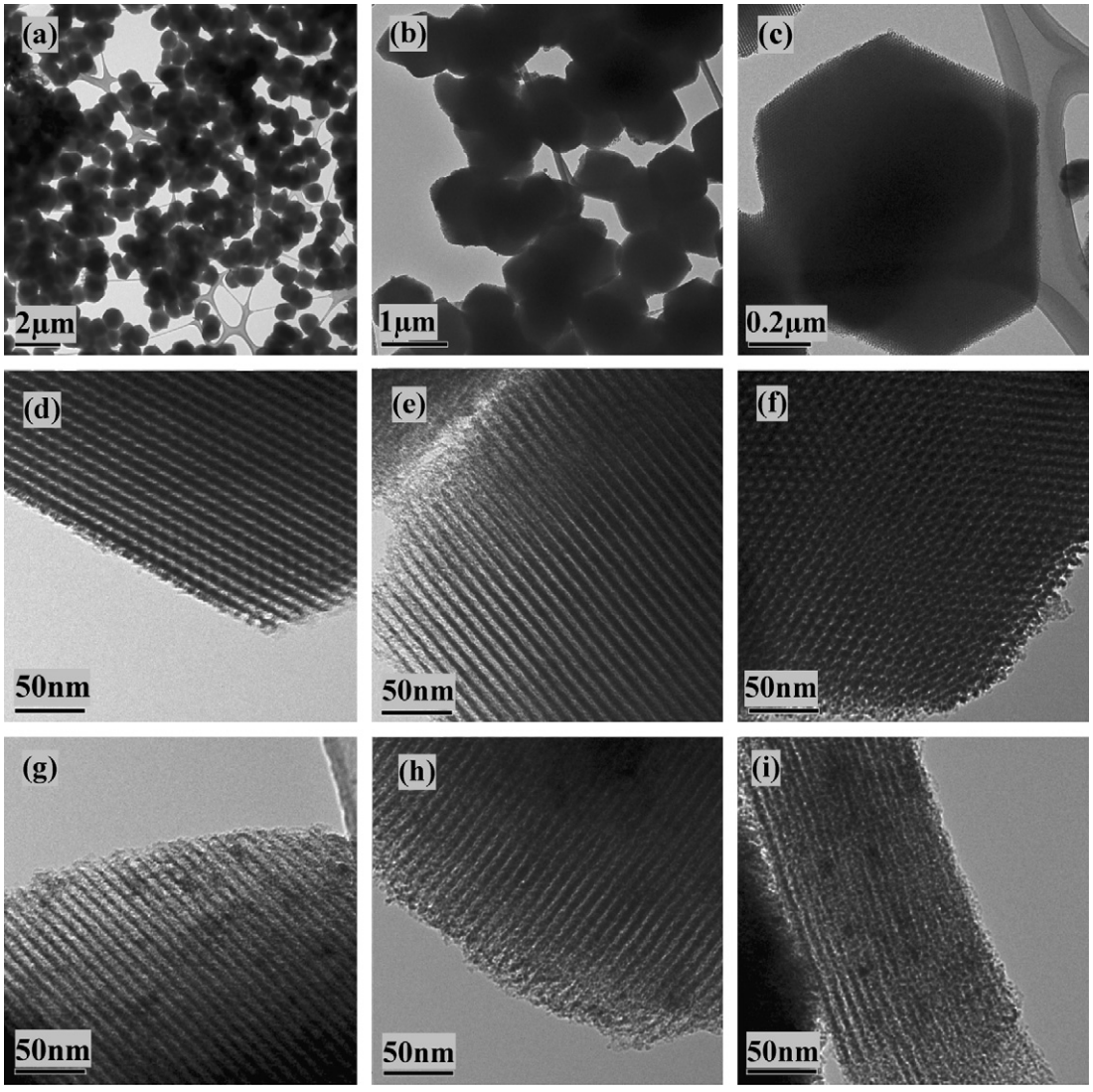

Fig. 3. The TEM images for low magnification SBA-15 structure (a–c), vanadium grafted 8.1V-SBA-15 (6.1 wt%) sample (d–f) and impregnated 6.0% V/SBA-15 sample (g–i).

maximum reduction rate to those of grafted V-SBA-15 catalyst with similar vanadium loadings; however, the integral peak area of the impregnated sample was much smaller than that of the grafted sample, suggesting that polymeric vanadium species deposited on the high-surface area SBA-15 support might be more difficult to reduce to the same valance with V-SBA-15 under the TPR conditions. The reduction temperature (806 K) for the impregnated catalyst (6.0V/SBA-15, 6 wt% V) was slightly (∼15 K) lower than the data reported by Fornés [23], likely due to the different temperature ramp rate and/or hydrogen concentration in the reducing stream during TPR.

3.1.5. Raman spectroscopy

Laser Raman spectroscopy was used to elucidate the molecular nature of vanadium domains. Although some have claimed that Raman spectroscopy may not be reliable for discriminating monomeric and polymeric vanadyl species [51], it still can be used to identify crystalline V_2O_5. The Raman spectra of dehydrated V-SBA-15 samples with different vanadium loadings are shown in Fig. 5, along with samples prepared by conventional wet impregnation. The silica support exhibits Raman features at 800 cm^{-1} (siloxane bridges), 480 and 600 cm^{-1} (three- and fourfold siloxane rings), and 980 cm^{-1} (surface silanol groups) [10]. A sharp Raman band at ∼1040 cm^{-1}, which has been assigned to the symmetric V=O stretching vibration of isolated VO_4 species [10,19], can be seen for the V-SBA-15 samples (spectra b–f), with increased intensity with increasing vanadium loading. The intensity of the two broad bands at ∼1070 and ∼915 cm^{-1} increased with the vanadium loading. These two bands, which are characteristics of Si–O^- and Si(–O^-)$_2$ functionalities [7,52] corresponding to the perturbation in silica vibrations, may be an indication of the V–O–Si formation. Its increasing intensity with the V loading suggests that more V–O–Si is formed during the grafting process, consuming more Si–OH hydroxyl groups. No significant band at ∼141 cm^{-1} corresponding to crystalline V_2O_5 could be observed even with the V-SBA-15 with the highest vanadium loading (21.6V-SBA-15, 9.2 wt%). The absence of a typical band at 995 cm^{-1} of

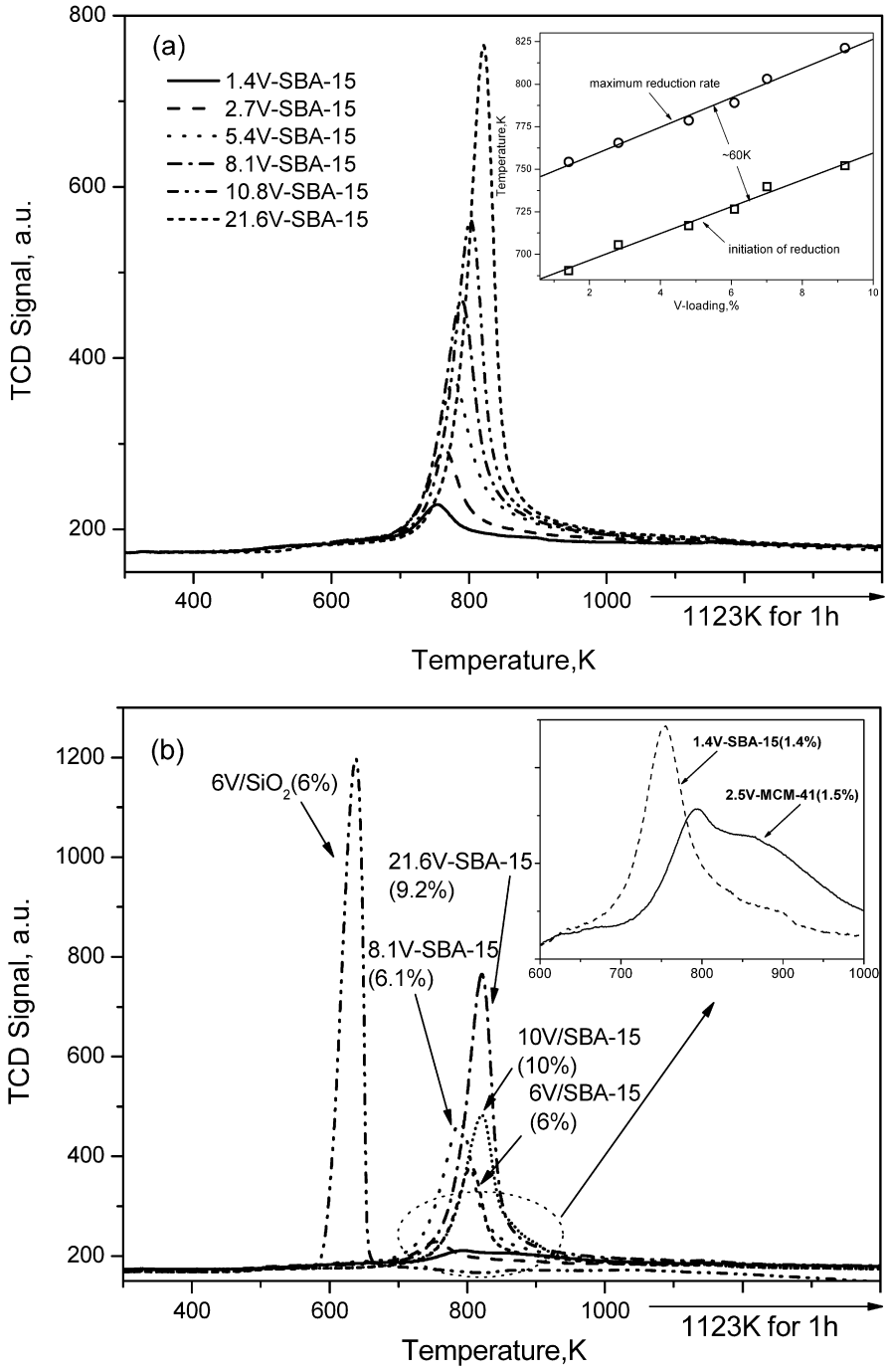

Fig. 4. Temperature programmed reduction (TPR) results of (a) grafted V-SBA-15 with different vanadium loading and (b) the comparison of V-SBA-15 with V-MCM-41, V/SBA-15, and V/SiO_2 samples.

V_2O_5 in spectra b–f implies that no polymeric crystalline V_2O_5 was formed in the grafted V-SBA-15 samples. These observations suggest that the vanadium domains on the surface all existed in an isolated environment, without aggregation to form crystalline V_2O_5. Similar Raman spectra pattern have been reported elsewhere for the vanadia-silica with relatively low vanadium loadings through the direct grafting of two precursors, $OV[OSi(O\,^tBu)_3]_3$ and $OV(O\,^tBu)_3$ [17].

All of the V_2O_5 characteristic Raman bands can be clearly observed for the V/SiO_2 samples (6 and 10 wt%), showing a series of peaks at 995, 698, 527, 482, 407, 302, 282, 194, and 141 cm^{-1}. The band located at 995 cm^{-1} is due primarily to the symmetric stretch of V=O groups in the vanadium oxide bulk [53]. A broad shoulder at ~1020 cm^{-1} was observed beside the sharp ~993 cm^{-1} band. For the vanadium-impregnated SBA-15 catalysts, however, at relatively low vanadium loading (6.0 wt%), only a band at ~1040 cm^{-1} could be seen as a characteristic of the V=O isolated species on the surface, due to the high surface area of mesoporous SBA-15 support. This is consistent with the absence of the feature of crystallization in the

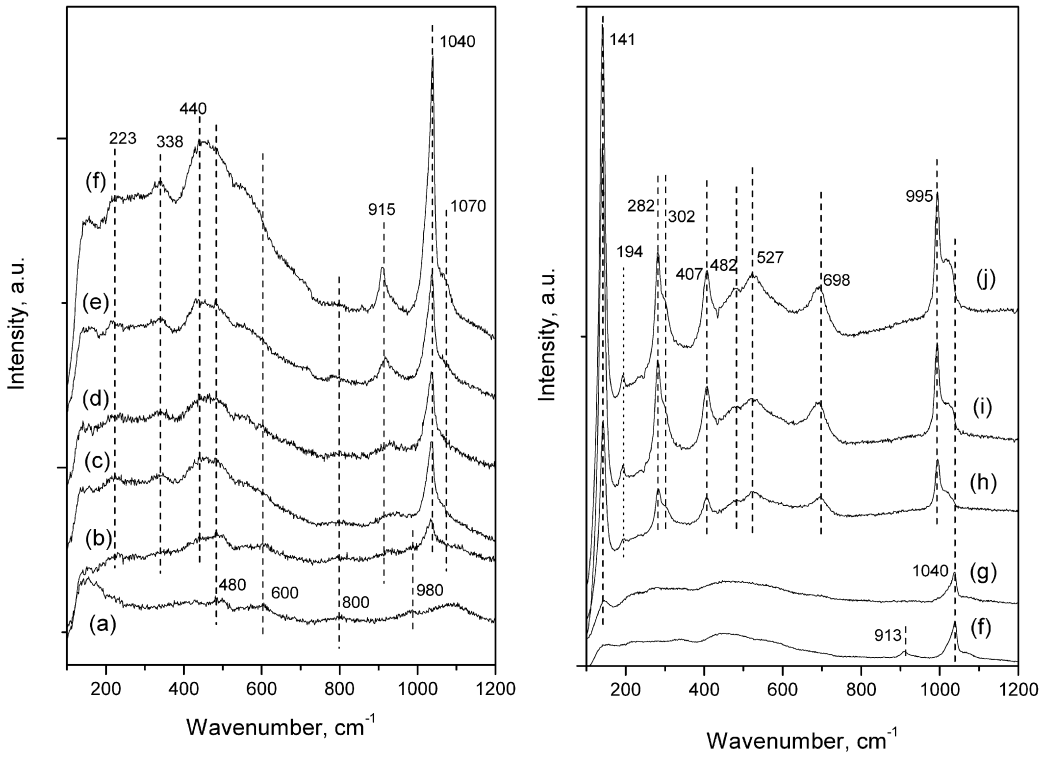

Fig. 5. Raman spectra of (a) SiO_2 (SBA-15), (b) 2.7V-SBA-15, (c) 5.4V-SBA-15, (d) 8.1V-SBA-15, (e) 10.8V-SBA-15, (f) 21.6V-SBA-15, (g) 6.0V/-SBA-15, (h) 10.0V/SBA-15, (i) 6.0%V/SiO_2, (j) 10.0%V/SiO_2.

XRD result for 6.0V/SBA-15. On the other hand, a weak Raman band appears at ∼141 cm^{-1}, which likely indicates a small amount of crystalline V_2O_5 is formed at this loading [7]. When the vanadium content is increased to 10.0 wt%, all the features of the crystalline V_2O_5-like structure were obtained, resulting in a similar Raman spectra with that of V/SiO_2 samples.

For the partially hydrated V-SBA-15 sample with high vanadium loading (21.6V-SBA-15, 10 wt%) and the vanadium impregnated SBA-15 sample (6.0%V/SBA-15) as shown in Fig. 6, some characteristic broad bands were seen at ∼702, ∼509, ∼271, and ∼154 cm^{-1}, which have been assigned to hydrated amorphous polymeric vanadium oxide species [10]. However, each spectrum exhibited a sharp peak at ∼1040 cm^{-1} instead of a broad band at ∼1020 cm^{-1} as another characteristic band of V_2O_5-like species, which might indicate that the V=O isolated structure can be substantially sustained by the introduction of H_2O molecules. Bonding of the H_2O molecule to the center V atom only changed the domain size by changing the coordination number, or aggregated the neighboring vanadium center to form V–O–V bonds. The 6.0%V/SiO_2 hydrated sample showed similar spectra with the dehydrated sample with V_2O_5 surface structure (not shown here), indicating that hydration in ambient condition did not change the local structure of the impregnated sample at this loading (6.0 wt%) because of the already-occupied polymeric vanadium crystalline domain with square pyramidal environment. Nevertheless, these characteristics were not significantly present in the V-SBA-15 with relatively low loading (8.1V-SBA-15, 6.1 wt%). This result indicates that at similar vanadium loadings, the grafted sample was more structurally stable against polymerization compared with the impregnated sample on hydration.

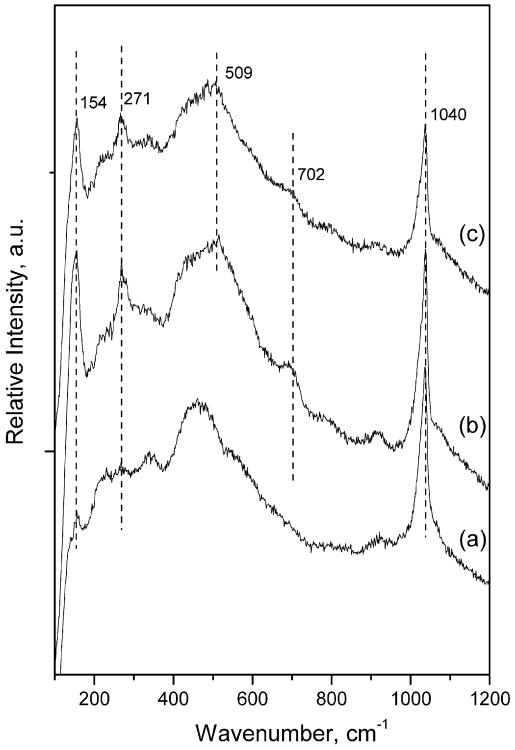

Fig. 6. Raman spectra of hydrated samples (a) 8.1V-SBA-15, (b) 21.6V-SBA-15, (c) 6.0V/SBA-15.

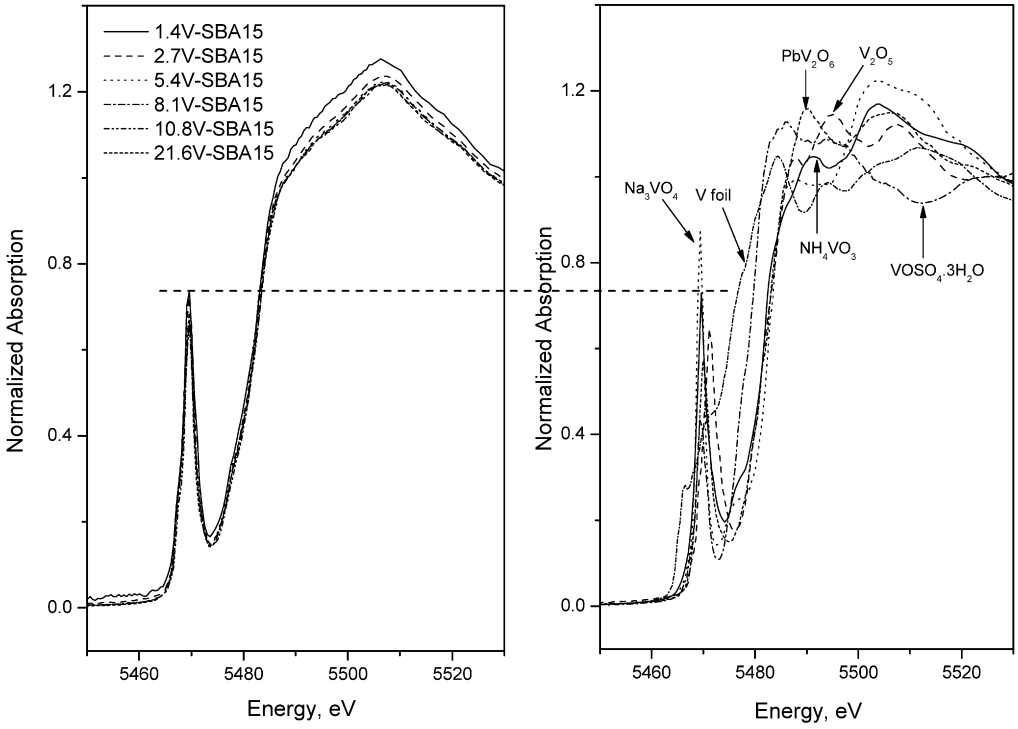

Fig. 7. Comparison of vanadium K-edge XANES regions for V grafted SBA-15 catalysts and the reference compounds.

3.1.6. XANES

The first-row transition metal elements exhibited well-defined site symmetry spectra in the XANES analysis. Normalized V K-edge XANES spectra of dehydrated vanadium-grafted SBA-15 catalyst and the vanadium reference compounds as well as vanadium metal foil are shown in Fig. 7. The standard edge energy was calibrated at the first inflection point (K-edge) in the foil calibration spectrum (5465.0 eV), which measures the threshold of photoejection of the 1 s electron in vanadium metal. The spectra of Fig. 7 show that the V K-edge XANES in the samples exhibit a pre-edge absorption feature corresponding to the forbidden transition 1s → 3d [46], which is caused mainly by mixing of 4p orbitals of vanadium atoms and 2p orbitals of the oxygen atoms with the 3d π orbitals of vanadium atoms [46]. The XANES regions for all of the V-SBA-15 samples are indistinguishable, indicating that they may exhibit the same electronic structures and site symmetries.

The XANES results on vanadium-grafted samples and reference compounds are summarized in Table 2. It is known that the pre-edge height and intensity are closely related to the local symmetry type, and they can be used to gain insight into the coordination structure when comparing the model compounds with a known coordination environment. The height of the pre-edge peak decreases monotonically as the vanadium structure changes from tetrahedral coordination to the square pyramidal or octahedral coordination. As shown in Fig. 7, the local symmetry of the vanadium domain in the V-SBA-15 samples had a smaller pre-edge height compared with the reference compound Na_3VO_4 (tetrahedral) and similar pre-edge height to NH_4VO_3 (distorted tetrahedral), suggesting a distorted tetrahedral coordination for the grafted samples with various vanadium loadings. It is observed that the pre-edge height decreased slightly with increasing vanadium loading; however, it still was much higher than that of the octahedral coordination species compared with PbV_2O_6. The distance between the pre-edge peak and the main edge is a measurement of the oxidation state of vanadium [46]. The E_{edge}–$E_{pre\text{-}edge}$ value has been reported to be between 12.4 and 12.8 for the tetrahedral vanadium(V) species, compared with 9.5 eV for the square pyramidal vanadium (V) as in V_2O_5 [46]. For compounds with lower oxidation states, this value decreased significantly as for $VOSO_4{\cdot}3H_2O$ (E_{edge}–$E_{pre\text{-}edge}$ = 8.4 eV). For the energy difference of the pre-edge peak to the main edge position as shown in Table 2, the E_{edge}–$E_{pre\text{-}edge}$ of the grafted samples varied from 11.6 to 13.0 eV, suggesting a tetrahedral coordination V(V) species. This value is much larger than that of V_2O_5 with a square pyramidal coordination, which excludes the existence of measurable aggregated vanadium oxides on the surface. This result suggests that the structure of vanadium clusters in V-SBA-15 is most likely distorted tetrahedron, which does not significantly change with vanadium loading up to the limit of monolayer coverage. The XANES results suggests that the samples synthesized through a grafting method preserve a local structural uniformity, and the increase of V-loading does not result in serious aggregation of the vanadium species on the SBA-15 wall surface. This result is consistent with Raman results showing the presence of only monomeric vanadium species on the SBA-15 surface under dehydrated conditions.

Empirically, the strength of the pre-edge transition has been found to be related to the size of the "molecular cage" [46]. Wong et al. [46] illustrated the correlation of the pre-edge intensity (defined by the height ∗ width at half-height) of different vanadium compounds and the domain size within the same symmetry quantitatively, suggesting an inverse molecular

Table 2
Energy positions of various spectral features in the V K-edge XANES spectra

Sample ID	Pre-edge peak position[a] (eV)	Main-edge position[a,b] (eV)	$E_{pre\text{-}edge}-E_0$ (eV)	$E_{edge}-E_{pre\text{-}edge}$ (eV)	Pre-edge peak height (a.u.)	Pre-edge peak intensity[c] (a.u.)
Na_3VO_4	5469.4	5482.1	4.4	12.7	0.87	1.60
NH_4VO_3	5469.6	5481.1	4.6	11.5	0.73	2.06
PbV_2O_6	5469.9	5481.4	4.9	11.5	0.57	1.71
V_2O_5	5471.1	5481.2	6.1	10.1	0.64	2.42
$VOSO_4{\cdot}3H_2O$	5469.3	5477.7	4.3	8.4	0.43	1.17
1.4V-SBA15D[d]	5469.6	5482.6	4.6	13.0	0.74	2.28
2.7V-SBA15D[d]	5469.5	5481.9	4.5	12.4	0.72	1.99
5.4V-SBA15D[d]	5469.7	5481.3	4.7	11.6	0.67	1.93
8.1V-SBA15D[d]	5469.6	5481.4	4.6	11.8	0.68	2.02
10.8V-SBA15D[d]	5469.6	5481.5	4.6	11.9	0.67	1.70
21.6V-SBA15D[d]	5469.4	5481.4	4.4	12.0	0.65	1.86
2.5V-MCM41D[d]	5469.7	5482.3	4.7	12.6	0.72	2.15
6.0I-VSBA15D[d]	5469.4	5481.1	4.4	11.7	0.68	2.02

[a] The uncertainty in peak positions is estimated to be ±0.2 eV.
[b] Main edge position is chosen as the mid point of absorption jump.
[c] Peak intensity is calculated by peak height ∗ width at half maximum.
[d] Samples were dehydrated in He at 623 K for 30 min before measurements.

cage–pre-edge absorption intensity relationship. The pre-edge peak intensity results for a series of V-SBA-15 samples summarized in Table 2 indicate that the pre-edge intensities of the samples, especially those with relatively low metal loading, resemble that of NH_4VO_3 with a distorted tetrahedral coordination, demonstrating that the vanadium domains of the V-SBA-15 samples are of a similar cage size as those of NH_4VO_3.

It was previously mentioned that a color change (from white or light yellow to dark yellow) occurred when the samples with vanadium grafted on the surface were exposed to ambient conditions. This change on hydration can be directly compared for the V K-edge spectra in the XANES region. A typical XANES spectrum of the V-SBA-15 sample (1.4 wt%) is illustrated in Fig. 8, and the comparisons of the pre-edge feature between the dehydrated and hydrated samples as a function of vanadium content are shown in Fig. 9. The pre-edge heights of hydrated vanadium grafted samples are smaller than those of the dehydrated samples, suggesting that the local structure of vanadium surface species may change from mostly tetrahedral coordination to partially octahedral coordination due to the absorbed H_2O. As shown in Fig. 8, a dramatic difference in the pre-edge feature can be observed, including a slight shift in the pre-edge position and a relative increase in the 1s → 4p transition above the edge at 5488.2 eV for the sample on hydration. As shown in Fig. 9, both the pre-edge heights and intensities decrease on hydration, suggesting an increase in the domain size or the change of coordination from distorted tetrahedron for the hydrated samples to distorted octahedron or polymeric vanadium structure with a V–O–V bridge, further confirming the Raman results on the hydration effect.

The redox properties of the V-SBA-15 catalyst were studied by in situ X-ray absorption. As shown in Fig. 10, reduction at 473 K in pure H_2 for 30 min did not change the pre-edge features of the dehydrated V-SBA-15 sample. With an increase in reduction temperature to 623 K, the pre-edge peak height decreased only slightly, from 0.67 of the fresh sample to 0.61,

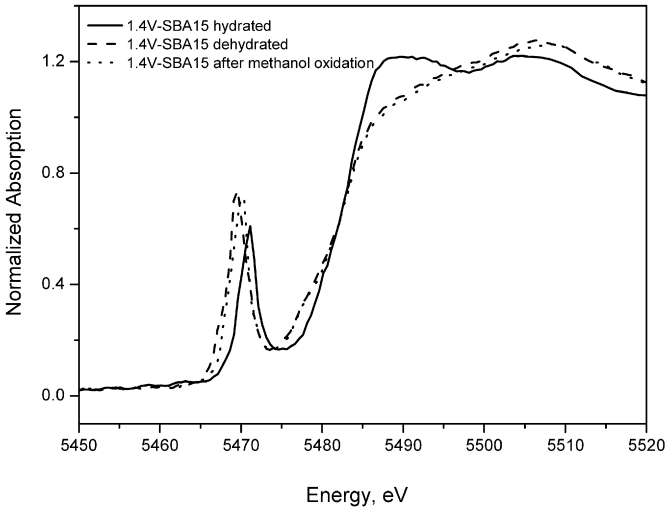

Fig. 8. Comparison of V K-edge XANES regions for dehydrated/hydrated samples and sample after methanol oxidation.

indicating that the local structure largely retained its tetrahedral coordination. The vanadium-grafted sample shows resistance to reduction up to 623 K under pure H_2 atmosphere. An increase in the reduction temperature to 773 K produced a dramatic decrease in the pre-edge peak. The shift of the main edge to lower energy indicates the reduction of vanadium from 5^+ to approximately 4^+ ($E_{edge}-E_{pre\text{-}edge} = 8.9$ eV) compared with the main edge position of $VOSO_4{\cdot}3H_2O$ compound ($E_{edge}-E_{pre\text{-}edge} = 8.4$ eV). As in the TPR profile of 10.8V-SBA-15, the vanadium reduction started at 740 K. It is reasonable to deduce that vanadium grafted on the surface of SBA-15 can be reduced only to 4^+ under the H_2-TPR conditions and remains in a square pyramidal coordination, without further reduction to lower valance or vanadium metal. After reoxidation in air at 773 K for 30 min, interestingly, the pre-edge peak increased to the level of the fresh sample, suggesting a return of the local structure to the distorted tetrahedral coordi-

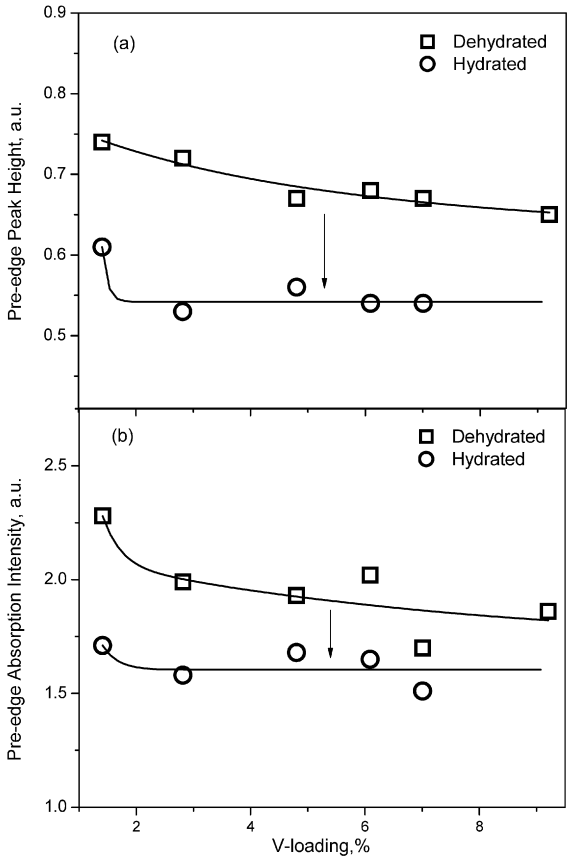

Fig. 9. Comparison of the pre-edge features including (a) pre-edge peak height and (b) pre-edge intensity of hydrated and dehydrated samples.

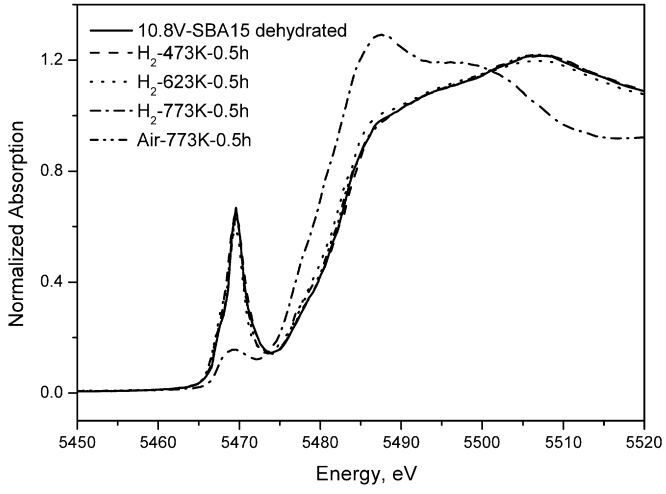

Fig. 10. In situ XANES study of the reducibility of V-SBA-15 sample (10.8V-SBA-15).

nation and the reconstruction of the Si–O–V bonds on the silica surface after the high-temperature air treatment. This likely suggests that after reduction at 773 K, the vanadium species changed from the original three-legged $(\equiv SiO)_3V{=}O$ to two-legged $(\equiv SiO)_2V{=}O$ species, accompanying the decrease in valance of V from 5^+ to 4^+. At 773 K, the two-legged V species is more stable than the three-legged V species, and the vanadium is not likely to undergo further reduction to 3^+. Thus,

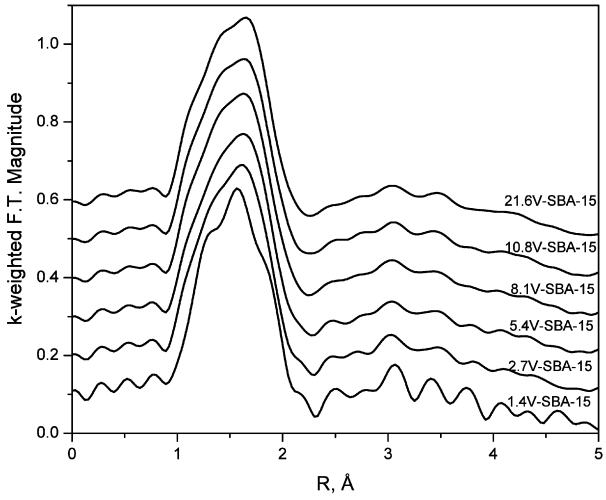

Fig. 11. Fourier transformed k^1-weighted EXAFS of vanadium grafted SBA-15: (a) 1.4V-SBA-15; (b) 2.7V-SBA-15; (c) 5.4V-SBA-15; (d) 8.1V-SBA-15; (e) 10.8V-SBA-15; (f) 21.6V-SBA-15.

when the V species is reoxidized at the sample temperature, the V–O–Si bond is reformed, resulting in reconversion to the tetrahedral coordination. Therefore, the vanadium grafted on the silica surface does not aggregate at the reduction condition, and maintains its isolated site.

3.1.7. EXAFS

EXAFS can provide quantitative information about the atomic structure and ligand environment. Fig. 11 compares the Fourier-transformed k^1-weighted EXAFS findings for the V-SBA-15 samples. The spectra are quite similar in the range of 1–3 Å, indicating similar first coordination spheres for vanadium species. The size of the vanadium complex on the silica surface was determined from the EXAFS spectra fitted, considering only the first-shell V–O coordination number with average V–O bond length for all of the samples, as summarized in Table 3. The average V–O coordination number varied from 3.8 to 4.5, suggesting that the V ions were grafted mostly on the silica surface tetrahedrally, confirming the proposed VO_4 model, without formation of aggregated vanadium species (i.e., V–O–V). To reduce the number of independent variables in the fit, coordination numbers were subsequently fixed at the fixed integer values of coordination, considering the well-accepted isolated VO_4 model with a terminal V=O and three bridging V–O bonds. The fitted parameters of the first two V–O shells are also listed in Table 3. The fitted distances of V=O (1.54 Å) and V–O (1.74 Å) were consistent with values reported previously [36,54]. Fig. 12 shows the agreement of the FT and fit for a typical vanadium-grafted sample (8.1V-SBA-15).

3.2. Catalyst performance in methanol oxidation

The activities of the V-SBA-15 catalysts were explored under steady-state conditions with constant flow rate (78 ml/min) and reaction pressure (2.5 psi) and a feed composition of 1.9 vol% methanol, 2.7 vol% of oxygen, and 95.4 vol% helium. Fig. 13 shows the conversion of methanol, selec-

Table 3
EXAFS initial fit results considering the average first shell and the fit of VO^{4-} model of two oxygen shells (terminal and bridging)

Sample ID	Average first oxygen shell				Two oxygen shells					
	CN	R (Å)	σ^2 (Å^2)	R factor	V=O CN	R (Å)	V–O CN	R (Å)	σ^2 (Å^2)	R factor
1.4V-SBA15D	4.54 ± 0.54	1.729	0.00938	0.006	1	1.544	3	1.739	0.00005	0.005
2.7V-SBA15D	4.00 ± 0.40	1.740	0.00778	0.006	1	1.542	3	1.737	0.00013	0.005
5.4V-SBA15D	3.78 ± 0.38	1.744	0.00703	0.006	1	1.543	3	1.738	0.00020	0.005
8.1V-SBA15D	3.94 ± 0.43	1.740	0.00782	0.007	1	1.542	3	1.737	0.00043	0.006
10.8V-SBA15D	3.95 ± 0.46	1.740	0.00836	0.008	1	1.542	3	1.737	0.00091	0.006
21.6V-SBA15D	3.85 ± 0.39	1.744	0.00752	0.006	1	1.544	3	1.738	0.00053	0.005
2.5-VMCM41D	4.04 ± 0.45	1.738	0.00787	0.007	1	1.542	3	1.737	0.00013	0.005
6.0IV/SBA15	3.90 ± 0.44	1.743	0.00881	0.006	1	1.543	3	1.737	0.00157	0.006

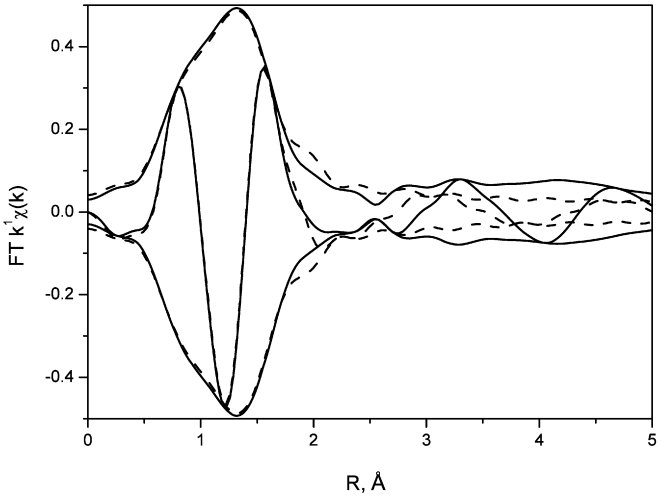

Fig. 12. k^1-weighted Fourier transform of the experimental $\chi(k)$ (solid) and the calculated fit (dashed) in R space for the first two shells.

tivity of formaldehyde and dimethyl ether, and space-time yield (STY_{HCHO}) of the vanadium-grafted samples with different vanadium loadings in terms of reaction temperature for the methanol oxidation reaction. Clearly, the conversion of methanol depends strongly on the vanadium content and reaction temperature. For 1.4V-SBA-15 with the lowest vanadium loading, methanol conversion increased slowly with increasing temperature up to 623 K, then rapidly thereafter. With increased vanadium loading in the V-SBA-15 samples, the methanol conversion profiles show a more significant trend with respect to reaction temperature, exhibiting a much lower "initiation" temperature for the "jump" in conversion. In other words, the clear increase in conversion shifted to lower temperatures with the increase in active sites. For the V-SBA-15 samples with higher vanadium loading, the methanol conversion approached 100%, and the temperature for the maximum conversion decreased with increasing vanadium loading. At high temperature, the effect of the vanadium loading on the methanol conversion decreased due to the high activity of the isolated active sites and the nearly complete consumption of the methanol in the feed, as shown in the inset of Fig. 13.

When the vanadium content exceeds the dispersion-limit loading (e.g., the monolayer capacity), aggregated species predominate [55,56]. The grafting mechanism that we propose in this work is the exchange of the ethoxyl groups of the intermediate $(EtO)_3V{=}O$ with $Si{-}O^-$ of the surface silanol groups, ideally forming three Si–O–V bonds per vanadium domain on the SBA-15 surface. This limits the maximum coverage of vanadium species grafted on the SBA-15 surface to be well below the monolayer (1.33 VO_x/nm^2, considering the estimated 4.0 $Si{-}OH/nm^2$ silanol group density [57]), no matter how high the concentration of the metal precursor used. We have demonstrated that a maximum of 9.2 wt% vanadium on the SBA-15 (21.6V-SBA-15) could be achieved with a nominal surface vanadium density of 1.06 VO_x/nm^2, due to the high surface area of SBA-15, as is clearly shown in Fig. 14. Thus, for all of the V-SBA-15 samples synthesized in this work, the monotonic increase in activity with increasing vanadium content in the temperature range studied indicates that the V-SBA-15 samples were all within the dispersion-limit loading without aggregating to polymeric vanadium species, which is consistent with the Raman and XANES results discussed above.

The formaldehyde selectivity profiles shown in Fig. 13b demonstrate significant differences with respect to vanadium loading. For samples with low vanadium content (<3.0 wt%), the selectivity increased with temperature within the 100-K range. Increasing the vanadium loading in the samples produced maximum formaldehyde selectivity within the temperature range studied and decreased the temperature of the greatest HCHO selectivity. This phenomenon was previously observed for V-MCM-41 catalysts on methane partial oxidation to formaldehyde [28]. This has been suggested to be related to the increase in highly dispersed isolated active sites with increased vanadium loading, which has a pre-exponential effect on the rate constant for the reaction, as we discussed in detail in previous work [58]. Due to the consecutive oxidation of the formaldehyde to carbon oxides for this series reaction, decreased selectivity with increasing temperature can be expected. The 21.6V-SBA-15 (9.2 wt% V) exhibited the highest formaldehyde selectivity of 86% at 598 K, due to its highest surface vanadium active site density.

As a major hydrocarbon product of methanol oxidation, the selectivity of dimethyl ether (DME) is demonstrated in Fig. 13c. This indicates the presence of acidic sites on V-SBA-15 catalysts. Interestingly, no DME was observed for the blank SBA-15 support. The DME selectivity profiles demonstrate that high temperature and high vanadium loading decreased the DME

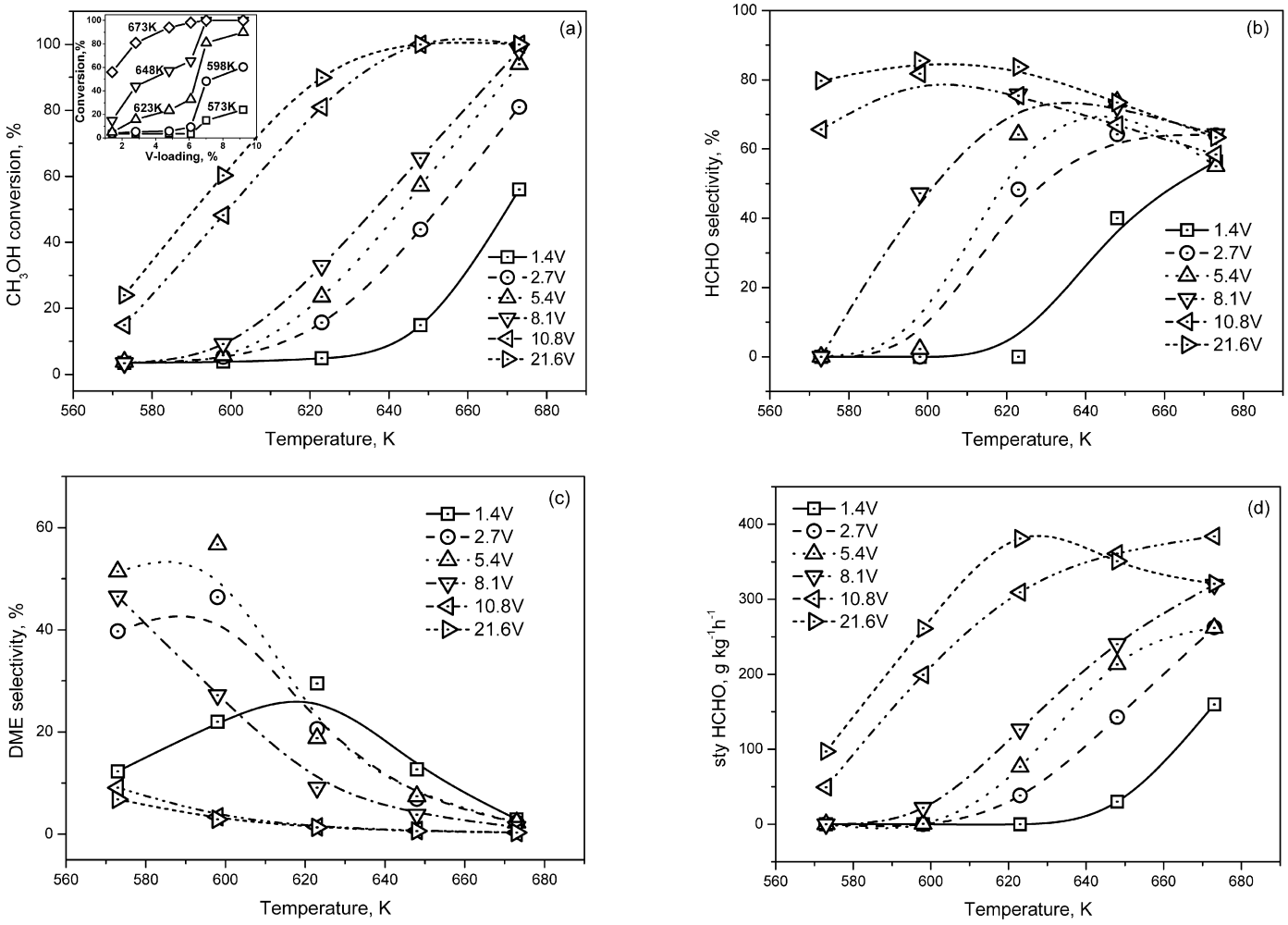

Fig. 13. Conversion of methanol (a), selectivity of formaldehyde (b) and dimethyl ether (c), and space time yield of formaldehyde (d) as a function of reaction temperature on V-SBA-15 catalysts with different vanadium content. (Reaction conditions: flow rate 78 ml/min, 1.9 vol% CH_3OH:2.7 vol% O_2:95.4 vol% He, pressure 2.5 psi.)

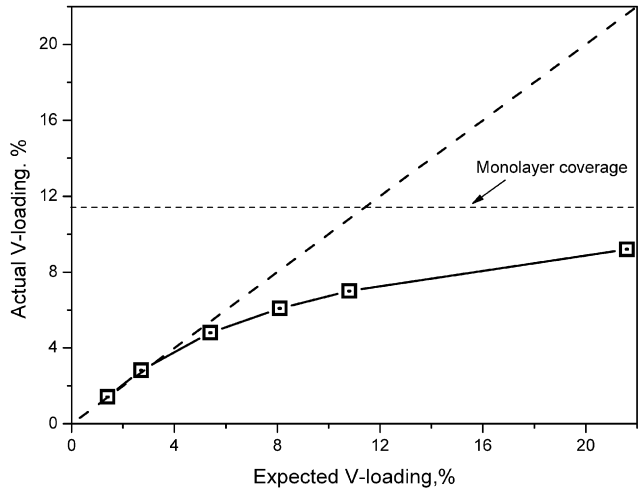

Fig. 14. The expected calculated V-loading compared to the actual vanadium that grafted on the SBA-15 surface.

selectivity, indicating an inverse relationship between the vanadium active sites active in formaldehyde production and the acidic sites active in DME production.

Fig. 13c also plots the space-time yield of formaldehyde for the combination of methanol conversion and formaldehyde selectivity. The figure shows that the yield of formaldehyde increased monotonically with temperature for the samples with vanadium loading up to 7.0 wt%. For the 21.6V-SBA-15 with vanadium loading approaching monolayer coverage, the drop in STY_{HCHO} at that high temperature from 648 to 673 K may be related to the complete consumption of methanol (100% conversion) and the secondary oxidation of the intermediate HCHO to CO_x.

We also compared the catalytic properties of the grafted V-SBA-15 catalyst and the V/SBA-15 catalyst with similar vanadium content. As shown in Fig. 15, the grafted sample exhibited much higher activity in the temperature range studied and demonstrated the maximum formaldehyde selectivity at lower temperatures. Based on the Raman and XANES results, the 6.0V/SBA-15 (6.0 wt% V) catalyst surprisingly showed no features of polymeric vanadium, which means at this loading, isolated vanadium species can predominate due to the high surface area of SBA-15 ($\sim$1000 m^2/g). However, the dramatic difference in catalytic performance strongly suggests a

huge difference between the samples prepared through grafting and those prepared through impregnation, demonstrating differences in local environment and dispersion. The grafted samples had more isolated vanadium species than the impregnated samples, contributing to the catalytic reaction.

Table 4 compares the catalytic performance (activity, selectivity, TOFs) of highly dispersed vanadia supported on SBA-15 synthesized in this work and in similar work through a different synthesis approach on the same reaction [59]. Compared with that previous work, our HCHO selectivities are lower, but our catalysts exhibit much higher activity. The lower selectivities likely can be attributed to high conversion; when compared at the same conversion, the selectivities should be comparable or higher. The difference in the two sets of results may be explained by the higher surface area of SBA-15 support, resulting in slightly lower nominal vanadium surface density and thus highly dispersed vanadia species.

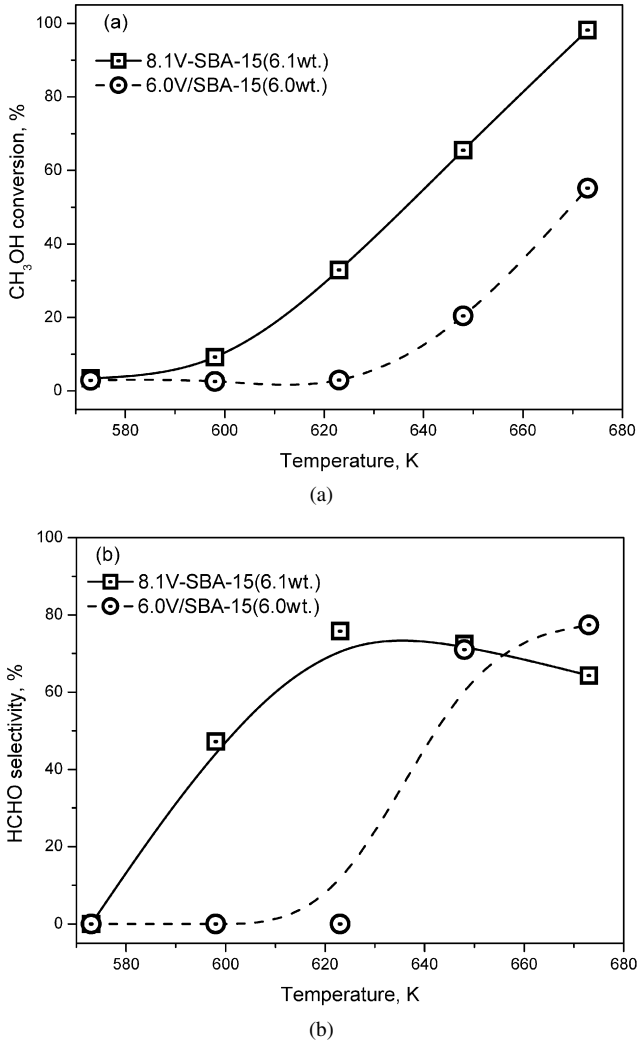

Fig. 15. Comparison of grafted V-SBA-15 catalyst and V/SBA-15 synthesized by conventional wet impregnation in terms of methanol conversion (a) and formaldehyde selectivity (b).

3.3. Acidic properties of V-SBA-15

The acidic properties of V grafted SBA-15 samples were investigated by pyridine TPD and compared with those of pure SBA-15. As shown in Fig. 16, the V-SBA-15 samples with different V-loading exhibited three pyridine desorption peaks at around 523, 653, and 823 K, indicating different acid sites of different acid strength on the surface of V-SBA-15. The broad signal at around 1000 K is due to the impurities during the synthesis of SBA-15. As reported by Lim and Haller in a study of the acidic properties of V-MCM-41 monitored by FTIR [60], the peak of pyridine TPD at relatively low temperature (523 K) may correspond to the Lewis acid sites, whereas the peaks at higher temperatures (653 and 823 K) may be attributed to Brönsted acid sites. The coexistence of both species of acid sites results in the formation of dimethylether. The numbers of both Lewis and Brönsted acid sites increase with increasing vanadium content grafted on the siliceous surface, accounting for the increased DME selectivity in methanol oxidation at low temperature.

It is generally agreed that the observation of DME as a product of methanol oxidation implies acidity in our V-SBA-15 catalysts, as has been confirmed and partially characterized by pyridine TPD. The fact that the acidity increases with V loading suggests that this acidity may be an inherent property of V embedded in silica for certain structures, but it is very difficult to rule out impurities. The fact that the acid site density correlates with V for both V-MCM-41 [60] and V-SBA-15 using different substrates, different V precursors, and different processes for incorporation/grafting might argue for an inherent acidity in some kinds of V sites. This is particularly true for the SBA-15, which appears to have no inherent acidity (see Fig. 16) but develops acidity progressively with in-

Table 4
Methanol oxidation to formaldehyde over highly dispersed vanadia supported on SBA-15

Sample ID	V (mmol/g)	VO_x (nm^2)	T (K)	MeOH/O_2/He (ml/min)	Conversion (MeOH)%	Selectivity (HCHO)%	TOF[a] ($\times 10^3$ s^{-1})	Reference
7.2% V/SBA-15	1.4	2.3	623	3/7/90	39.0	93.3	–	[59][b]
10.8V-SBA-15	1.37	1.16	623	2/3/95	81.0	75.4	2.1	This work
2.3% V/SBA-15	0.45	0.6	673	3/7/90	64–70%	88.1	11.2	[59][b]
2.7V-SBA-15	0.55	0.36	673	2/3/95	81.0	64.0	4.4	This work
7.2% V/SBA-15	1.4	2.3	673	3/7/90	64–70%	88.7	5.5	[59][b]
10.8V-SBA-15	1.37	1.16	673	2/3/95	100	58.4	2.6	This work

[a] Apparent TOF of HCHO is calculated by the number of moles of methanol converted to formaldehyde per mole of surface vanadium atom per second.
[b] A more completed summary of the catalytic performance of highly dispersed vanadia supported on various mesoporous silica materials can be found in the same reference.

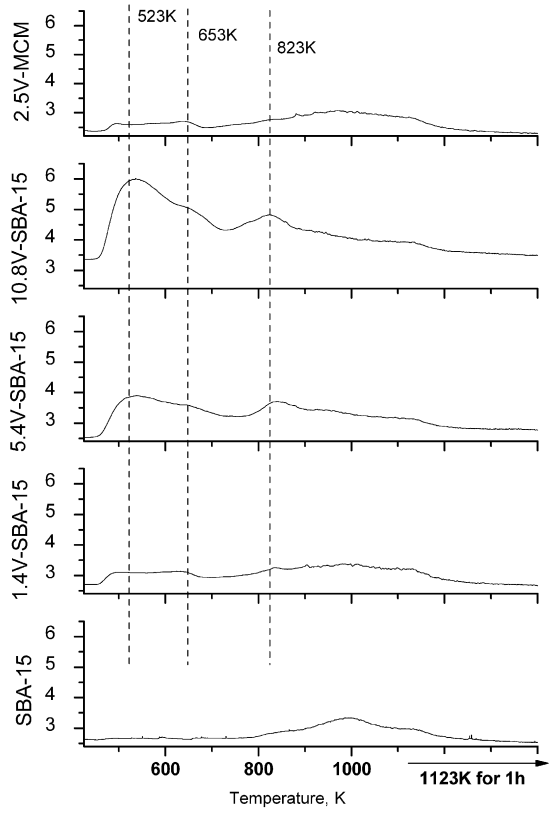

Fig. 16. Pyridine TPD patterns for V-MCM-41, SBA-15 and V-SBA-15 with different V-loadings.

creasing V loading, because the grafting process uses a very pure $O{=}VCl_3$ vanadium source that is then converted to the $O{=}V(CH_3CH_2O)_3$ precursor, a virtual purification process. On the other hand, we have prepared V-MCM-41 using an impure HiSil 233 silica course (and observed apparent acidity in the methanol oxidation) and a pure Cab-O-Sil source where no dimethyl ether was detected [15], suggesting that all acidity is associated with impurities or that acidity associated with V occurs only at certain (higher) loading in certain structures. The latter hypothesis, although not impossible, seems somewhat improbable. Putting aside the structure/source of acidity, we note that the 2.5V-MCM-41 (1.5 wt% V) has fewer acid sites than the 1.4V-SBA-15 (1.4 wt% V), according to Fig. 16. This again might argue for an impurity interpretation (which uncouples acid site density from V site density), but may reflect differing distributions of V in sites that do and do not impart acidity. Thus, we can neither confirm the possibility of inherently acidic V in silica sites nor identify the likely precursor if it is due to an impurity, and therefore must leave the description of the acid site as an open question.

4. Conclusion

We have successfully synthesized vanadium-grafted SBA-15 catalysts with various vanadium content by an atomic layer deposition method with high dispersions of isolated active sites. Using different characterization techniques, the active vanadium species have been assigned to isolated VO_4 sites with a terminal V=O bonds and three V–O bonds. The better activity of the V-SBA-15 catalysts compared with those synthesized by impregnation is attributed to the homogeneous dispersion of vanadium active single sites. The Lewis and Brönsted acid sites on the V-SBA-15 surface result in the production of DME.

Acknowledgments

This work was supported by grants from NASA (NAG 04) and the US DOE, Office of Basic Energy Sciences (DE-FG02-01ER15183). The authors thank the National Synchrotron Light Source at Brookhaven National Laboratory for providing beamtime for these experiments.

References

[1] U.S. Ozkan, T.A. Harris, B.T. Schilf, Catal. Today 33 (1997) 57.
[2] H. Bosch, F. Janssen, Catal. Today 2 (1988) 369.
[3] G.C. Bond, S.F. Tahir, Appl. Catal. 71 (1991) 1.
[4] G.A. Du, S. Lim, Y.H. Yang, C. Wang, L. Pfefferle, G.L. Haller, Appl. Catal. A 302 (2006) 48.
[5] A. Khodakov, B. Olthof, A.T. Bell, E. Iglesia, J. Catal. 181 (1999) 205.
[6] I.E. Wachs, B.M. Weckhuysen, Appl. Catal. A 157 (1997) 67.
[7] X.T. Gao, S.R. Bare, B.M. Weckhuysen, I.E. Wachs, J. Phys. Chem. B 102 (1998) 10842.
[8] G. Busca, G. Centi, L. Marchetti, F. Trifiro, Langmuir 2 (1986) 568.
[9] K. Inumaru, M. Misono, T. Okuhara, Appl. Catal. A 149 (1997) 133.
[10] N. Das, H. Eckert, H.C. Hu, I.E. Wachs, J.F. Walzer, F.J. Feher, J. Phys. Chem. 97 (1993) 8240.
[11] S. Irusta, L.M. Cornaglia, E.E. Miro, E.A. Lombardo, J. Catal. 156 (1995) 167.
[12] M. Iwamoto, J. Hirata, K. Matsukami, S. Kagawa, J. Phys. Chem. 87 (1983) 903.
[13] B. Olthof, A. Khodakov, A.T. Bell, E. Iglesia, J. Phys. Chem. B 104 (2000) 1516.
[14] J. Dobler, M. Pritzsche, J. Sauer, J. Am. Chem. Soc. 127 (2005) 10861.
[15] Y.H. Yang, G.A. Du, S.Y. Lim, G.L. Haller, J. Catal. 234 (2005) 318.
[16] J.M. Thomas, R. Raja, D.W. Lewis, Angew. Chem. Int. Ed. 44 (2005) 6456.
[17] D.A. Ruddy, N.L. Ohler, A.T. Bell, T.D. Tilley, J. Catal. 238 (2006) 277.
[18] M.M. Koranne, J.G. Goodwin, G. Marcelin, J. Catal. 148 (1994) 388.
[19] G.T. Went, S.T. Oyama, A.T. Bell, J. Phys. Chem. 94 (1990) 4240.
[20] C.B. Wang, R.G. Herman, C.L. Shi, Q. Sun, J.E. Roberts, Appl. Catal. A 247 (2003) 321.
[21] M.M. Koranne, J.G. Goodwin, G. Marcelin, J. Catal. 148 (1994) 369.
[22] H. Berndt, A. Martin, A. Bruckner, E. Schreier, D. Muller, H. Kosslick, G.U. Wolf, B. Lucke, J. Catal. 191 (2000) 384.
[23] V. Fornes, C. Lopez, H.H. Lopez, A. Martinez, Appl. Catal. A 249 (2003) 345.
[24] M. Baltes, K. Cassiers, P. Van Der Voort, B.M. Weckhuysen, R.A. Schoonheydt, E.F. Vansant, J. Catal. 197 (2001) 160.
[25] D. Wei, H. Wang, X.B. Feng, W.T. Chueh, P. Ravikovitch, M. Lyubovsky, C. Li, T. Takeguchi, G.L. Haller, J. Phys. Chem. B 103 (1999) 2113.
[26] S. Lim, G.L. Haller, J. Phys. Chem. B 106 (2002) 8437.
[27] Y.H. Yang, S. Lim, C. Wang, D. Harding, G. Haller, Microporous Mesoporous Mater. 67 (2004) 245.
[28] G.A. Du, S.Y. Lim, Y.H. Yang, C. Wang, L. Pfefferle, G.L. Haller, Appl. Catal. A 302 (2006) 48.
[29] C. Coperet, M. Chabanas, R.P. Saint-Arroman, J.M. Basset, Angew. Chem. Int. Ed. 42 (2003) 156.
[30] T.D. Tilley, J. Mol. Catal. A Chem. 182 (2002) 71.
[31] G.L. Rice, S.L. Scott, J. Mol. Catal. A Chem. 125 (1997) 73.
[32] G.L. Rice, S.L. Scott, Langmuir 13 (1997) 1545.
[33] W. Priebsch, D. Rehder, Inorg. Chem. 29 (1990) 3013.

[34] E.C.E. Rosenthal, F. Girgsdies, Z. Anorg. Allg. Chem. 628 (2002) 1917.
[35] N.N. Ghosh, J.C. Clark, G.T. Eldridge, C.E. Barnes, Chem. Commun. (2004) 856.
[36] F.J. Feher, J.F. Walzer, Inorg. Chem. 30 (1991) 1689.
[37] O.B. Lapina, M.A. Mats'ko, T.B. Mikenas, V.A. Zakharov, E.A. Paukshtis, D.F. Khabibulin, A.P. Sobolev, Kinet. Catal. 42 (2001) 553.
[38] E.W. Deguns, Z. Taha, G.D. Meitzner, S.L. Scott, J. Phys. Chem. B 109 (2005) 5005.
[39] K.L. Fujdala, T.D. Tilley, Chem. Mater. 14 (2002) 1376.
[40] K.L. Fujdala, T.D. Tilley, J. Catal. 216 (2003) 265.
[41] D.Y. Zhao, Q.S. Huo, J.L. Feng, B.F. Chmelka, G.D. Stucky, J. Am. Chem. Soc. 120 (1998) 6024.
[42] D.Y. Zhao, J.L. Feng, Q.S. Huo, N. Melosh, G.H. Fredrickson, B.F. Chmelka, G.D. Stucky, Science 279 (1998) 548.
[43] J.E. Herrera, J.H. Kwak, J.Z. Hu, Y. Wang, C.H.F. Peden, J. Macht, E. Iglesia, J. Catal. 239 (2006) 200.
[44] S. Brunauer, P.H. Emmett, E. Teller, J. Am. Chem. Soc. 60 (1938) 309.
[45] E.P. Barrett, L.G. Joyner, P.P. Halenda, J. Am. Chem. Soc. 73 (1951) 373.
[46] J. Wong, F.W. Lytle, R.P. Messmer, D.H. Maylotte, Phys. Rev. B 30 (1984) 5596.
[47] E.A. Stern, M. Newville, B. Ravel, Y. Yacoby, D. Haskel, Physica B 209 (1995) 117.
[48] A.L. Ankudinov, B. Ravel, J.J. Rehr, S.D. Conradson, Phys. Rev. B 58 (1998) 7565.
[49] R. Schmidt, E.W. Hansen, M. Stocker, D. Akporiaye, O.H. Ellestad, J. Am. Chem. Soc. 117 (1995) 4049.
[50] A. Vinu, D.P. Sawant, K. Ariga, K.Z. Hossain, S.B. Halligudi, M. Hartmann, M. Nomura, Chem. Mater. 17 (2005) 5339.
[51] N. Magg, B. Immaraporn, J.B. Giorgi, T. Schroeder, M. Baumer, J. Dobler, Z.L. Wu, E. Kondratenko, M. Cherian, M. Baerns, P.C. Stair, J. Sauer, H.J. Freund, J. Catal. 226 (2004) 88.
[52] P. MacMillan, Am. Mineral. 69 (1986) 622.
[53] L. Abello, E. Husson, Y. Repelin, G. Lucazeau, Spectrochim. Acta Part A 39 (1983) 641.
[54] R. Rulkens, J.L. Male, K.W. Terry, B. Olthof, A. Khodakov, A.T. Bell, E. Iglesia, T.D. Tilley, Chem. Mater. 11 (1999) 2966.
[55] M. Faraldos, M.A. Banares, J.A. Anderson, H.C. Hu, I.E. Wachs, J.L.G. Fierro, J. Catal. 160 (1996) 214.
[56] M.A. Banares, J.H. Cardoso, F. Agullo-Rueda, J.M. Correa-Bueno, J.L.G. Fierro, Catal. Lett. 64 (2000) 191.
[57] I.G. Shenderovich, G. Buntkowsky, A. Schreiber, E. Gedat, S. Sharif, J. Albrecht, N.S. Golubev, G.H. Findenegg, H.H. Limbach, J. Phys. Chem. B 107 (2003) 11924.
[58] G.A. Du, Y. Yang, W. Qiu, S. Lim, L. Pfefferle, G.L. Haller, Appl. Catal. A 313 (2006) 1.
[59] C. Hess, I.J. Drake, J.D. Hoefelmeyer, T.D. Tilley, A.T. Bell, Catal. Lett. 105 (2005) 1.
[60] S.Y. Lim, G.L. Haller, Appl. Catal. A 188 (1999) 277.